PROCEEDINGS OF SCIENCE

A high granularity active target for the PIONEER experiment

Simone M. Mazza,[a,*] **M. Escobar,**[a] **G. Giacomini,**[b] **X. Qian,**[b] **B. A. Schumm,**[a] **A. Seiden,**[a] **R. Stern,**[a] **A. Molnar,**[a] **M. Nizam,**[a] **J. Ott,**[a] **T. Shin,**[a] **V. Tishchenko,**[b] **N. Yoho**[a] **and Y. Zhao**[a]

[a] *SCIPP, UC Santa Cruz,*
1156 High St, Santa Cruz (CA), U.S.
[b] *Brookhaven National Laboratories,*
P.O. Box 5000, Upton (NY), U.S.

E-mail: simazza@ucsc.edu

PIONEER is a next-generation experiment to measure the charged-pion branching ratio to electrons vs. muons and the pion beta decay with an order of magnitude improvement in precision. This will probe lepton universality at an unprecedented level and test CKM unitarity at the quantum loop level. PIONEER was approved in 2022 to run at the PiE5 pion beamline at PSI. A high-granularity active target (ATAR) is being designed to provide detailed 4D tracking information, allowing the separation of the energy deposits of the pion decay products in both position and time. The chosen technology for the ATAR is Low Gain Avalanche Detectors (LGAD). These are thin silicon detectors with moderate internal signal amplification. To achieve a 100% active region, prototype technologies under development are being evaluated, such as AC-coupled LGADs (AC-LGADs). Since a range of deposited charge from Minimum Ionizing Particle (MIP, few 10s of keV) from positrons to several MeV from the stopping pions/muons is expected, the detection and separation of close-by hits in such a wide dynamic range will be a challenge. Furthermore, the compactness and the requirement of low inactive material of the ATAR present challenges for the readout system, forcing the amplification chip and digitization to be positioned away from the active region. This paper will introduce PIONEER and the ATAR, then show a selection of R&D results on sensors and electronics.

10th International Workshop on Semiconductor Pixel Detectors for Particles and Imaging (Pixel2022)
12-16 December 2022
Santa Fe, New Mexico, USA

*Speaker

PoS(Pixel2022)015

1. Introduction

PIONEER [1, 2] is a next-generation pion decay experiment to measure $R_{e/\mu}$ and pion beta decay with an order of magnitude improvements in precision from the PIENU [3], PEN [4], and PIBETA [5] experiments. The PSI committee approved the experiment to take place at one of the pion beam lines (PiE1 or PiE5) at PSI in a timescale of 5 years. PIONEER will run in three phases: Phase I will be focused on lepton flavor universality, and Phase II and III will be focused on the measurement of V_{ud}.

The Phase I of PIONEER is a measurement of the helicity-suppressed ratio of pion decay rates $R_{e/\mu} = \frac{\Gamma(\pi^+ \to e^+\nu(\gamma))}{\Gamma(\pi^+ \to \mu^+\nu(\gamma))}$ which provides the most stringent test of Lepton Flavor Universality. In the Standard Model (SM), $R_{e/\mu}$ has been calculated with extraordinary precision at the 10^{-4} level as [6–8], perhaps the most precisely calculated weak interaction observable involving quarks. Because the uncertainty of the SM calculation for $R_{e/\mu}$ is minimal and the decay $\pi^+ \to e^+\nu$ is helicity-suppressed by the $V - A$ structure of charged currents, a measurement of $R_{e/\mu}$ is susceptible to the presence of pseudo-scalar (and scalar) couplings absent from the SM; a disagreement with the theoretical expectation would unambiguously imply the existence of new physics beyond the SM. PIONEER has the goal of 0.01% of experimental precision for $R^{\pi}_{e/\mu}$, which is an order of magnitude lower than the value (0.2%) reported by PIENU [9], reaching a precision comparable to the SM calculation. New physics beyond the SM (BSM) up to the mass scale of 3000 TeV may be revealed by a deviation from the precise SM expectation [8]. Searches for sterile neutrinos and other exotic reactions will also be pursued in Phase I.

PIONEER's Phases II and III will focus on the precision measurement of pion beta decay, $\pi^+ \to \pi^0 e^+ \nu(\gamma)$. Measurements of beta decay of neutrons, nuclei, and mesons provide very accurate determinations of the elements $|V_{ud}|$ and $|V_{us}|$ of the CKM quark-mixing matrix [10, 11]. Recent theoretical developments on radiative corrections and form factors have led to a 3σ tension with CKM unitarity, if confirmed, would point to new physics in the multi-TeV scale (see, e.g., Ref. [12]). The PiBeta experiment at PSI accurately measured the branching ratio for pion beta decay with a precision of 0.3% [13]. With current input, the experimental uncertainty of V_{ud} comes almost entirely from the $\pi^+ \to \pi^0 e^+ \nu(\gamma)$ branching ratio [14]. This makes $\pi^+ \to \pi^0 e^+ \nu(\gamma)$ irrelevant for the CKM unitarity tests because super-allowed nuclear beta decays provide a nominal precision of 0.03%. However, PIONEER aims to improve by one order of magnitude the precision of $\pi^+ \to \pi^0 e^+ \nu(\gamma)$, making it relevant for the CKM unitarity.

2. PIONEER experiment setup

To achieve the necessary precision for both $R_{e/\mu}$ and $\pi^+ \to \pi^0 e^+ \nu(\gamma)$ PIONEER has three main detectors: a high granularity fully active silicon target (in short ATAR), a 28 X_0 segmented calorimeter with high energy resolution, and a low mass tracker in-between. Currently, the detector designed is focused on phase I of the experiment ($R_{e/\mu}$) in which the two decays have a final positron with energy of 69 MeV for $\pi^+ \to e^+\nu(\gamma)$ or 0-53 MeV for $\pi^+ \to \mu^+\nu(\gamma)$. However, experimental broadening and pion/muon decays in flight cause the two spectra to overlap significantly for the target level of precision.

A mechanical drawing of PIONEER external enclosure is in fig. 1, left. A schematic of the experiment and pion decay path is shown in fig. 1, right. Based on Low Gain Avalanche Detectors (LGADs), the ATAR has a few mm of active thickness, fast charge collection time, and a few 100 μm of granularity in X, Y, Z. It sits at the most probable pion interaction point and provides a high precision 4D tracking for each pion decay event. This allows the separation of the energy deposits of the decay products in both position and time. Furthermore, it will allow the suppression of other significant systematic uncertainties (pulse pile-up, decay in flight of slow pions) to $< 0.01\%$. Based on LXe performance [15], the calorimeter will allow a few % precision on the exiting positron energy and complete containment of the shower. The low mass tracker provides a positron track to aid the recombination of events between ATAR and the Calorimeter. The combination of the high-precision calorimeter and the ATAR will allow the overall uncertainty in the measurements of $R_{e/\mu}$ and Pib to be reduced to O(0.01%) and O(0.05%), respectively. The following sections will be focused on ATAR sensors and electronics development.

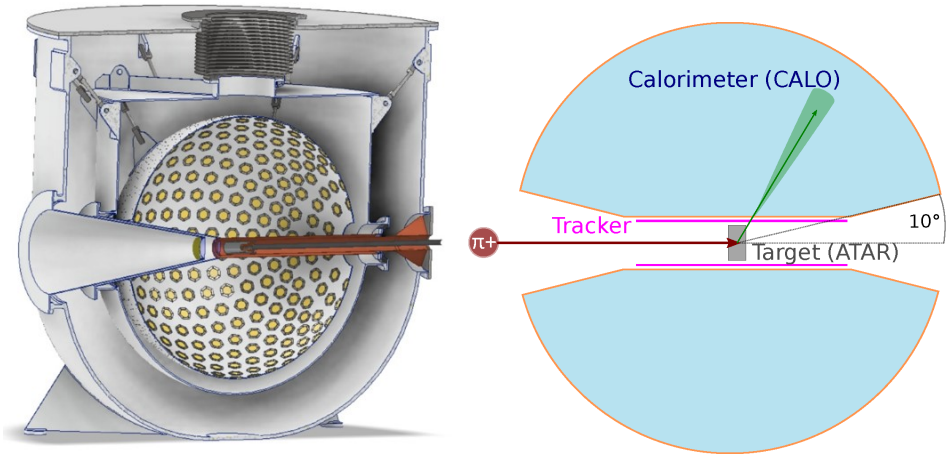

Figure 1: Left: External enclosure for PIONEER calorimeter and ATAR. Right: Pion decay schematic in the ATAR, tracker, and Calorimeter.

3. Active target (ATAR)

A silicon-based highly segmented active target (ATAR) is a key new feature of the PIONEER experiment. The goal of the ATAR is to enable pattern recognition capabilities to separate $\pi^+ \to e^+\nu$ decays from the $\pi^+ \to \mu^+(e^+\nu\bar{\nu})\nu$ decays. Ultimately, it is expected that ATAR will be able to suppress the $\pi \to \mu \to e$ chain by several orders of magnitude. Those events are identified using the ~1.5 ns pulse pair resolution of thin silicon sensors and a tight positron observation window of about one pion lifetime, which disfavors the slower muon decay. This reduces the number of muon decay electrons sufficiently, so that the low energy tail of the calorimeter π_{2e} response extending below the maximum Michel energy can be directly measured.

Furthermore it will limit accidental muon stops that precedes the trigger signal. These were a significant background in the previous generation of experiments and had to be suppressed by pile-up rejection at the expense of event rate. This can be achieved by checking whether the observed positron belongs to the pion stopping vertex using additional tracking detectors.

The ATAR will also identify decays in flight. Muons arising from upstream pion decays are relatively easily identified by their energy loss properties and by kinks in their trajectories. Pion decay inside the target will be separated by kinks in the topology, dE/dx along the track, and range in the target. The basic features of the signal and backgrounds are illustrated in fig. 2.

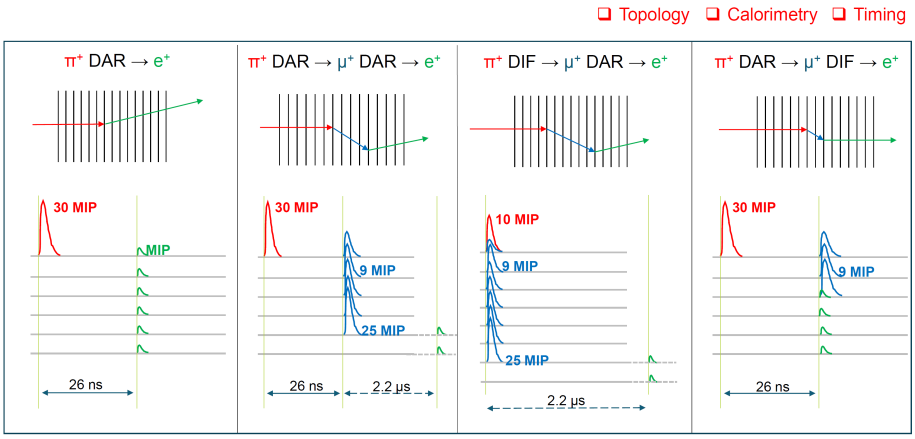

Figure 2: Illustration of the signatures of signal ($\pi^+ \to e^+\nu$) and different backgrounds ($\pi^+ \to \mu^+(e^+\nu\bar{\nu})\nu$). Topology information (2 vs. 3 tracks), timing information (26 ns vs. 26 ns + 2.2 μs) and energy information (10% difference in the energy deposition per unit length between μ and π).

To achieve the stated pion decay chain separation the ATAR requires:

- Excellent position resolution: there are two tracks (stopped π^+ and decay e^+) in the $\pi^+ \to e^+\nu$ decays, while there are three tracks (stopped π^+, stopped μ^+, and decay e^+) in the $\pi^+ \to \mu^+(e^+\nu\bar{\nu})\nu$ decays. With 4.2 MeV energy, the μ^+ in the latter case can, on average, travel 750 μm. Therefore, a position resolution of about 100 μm is essential.
- Excellent timing resolution for T_0 and two-hit separation: Given the pion lifetime of ~26 ns and the muon lifetime of ~2.2 μs, PIONEER requires identifying $\pi \to \mu$ hits separated by 1.5 ns. In addition, a sub-ns T_0 timing resolution is important to handle the 300 kHz rate and to reject μ and e^+ backgrounds in the beam.
- Excellent energy resolution: An excellent energy resolution is important to separate a stopped pion from a stopped muon, whose energy loss per unit length is separated by about 10%, as well as measure the energy loss of the decay positron.

To make the best use of the complex event topology of the ATAR, detailed signal processing, and advanced event reconstruction algorithms originated from the Wire-Cell event reconstruction developed for the Liquid Argon Time Projection Chamber (LArTPC) [16, 17], are being explored.

4. ATAR design

The ATAR dimensions are 2×2 cm^2 transverse to the beam. In the beam direction, individual silicon sensors are tightly stacked with a total thickness of roughly 6 mm. The requirement of avoiding dead material in the detector volume precludes the use of bump-bonded electronics

readout chips. For this reason, a strip geometry with the electronic readout connected on the side of the active region is foreseen. The strips are oriented at 90^0 to each other in subsequent staggered planes to provide a measurement of both coordinates of interest and allow space for the readout and wire bonds. In the design, the strips are wire bonded to a flex, alternating the connection on the four sides, which brings the signal to a readout chip positioned a few cm away from the active volume to be outside of the calorimeter acceptance. Then a second connection, which also provides the various voltages and grounds, brings the amplified signal to the digitizers in the back end.

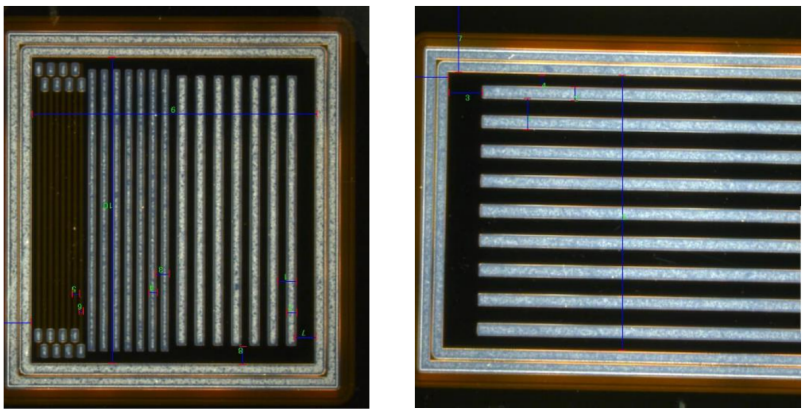

Figure 3: Photos of BNL prototype strip AC-LGADs. Left: a multi-pitch (300 μm, 200 μm, 100 μm) and width strip sensor with 0.5 cm of length (also studied with the same geometry and 1 cm length). Right: a 500 μm pitch sensor with 2.5 cm of length.

The foreseen sensor geometry has a pitch of 200 μm with 100 strips mated to a chip with 100 channels and 2 cm width, a standard dimension for microchips. The chosen baseline technology for the ATAR is based on Low Gain Avalanche Detectors (LGAD) [18], thin silicon detectors with moderate internal gain. Due to the internal gain and thin bulk, LGADs have a fast rise time and a short full charge collection time. The best estimate at present for the sensor thickness is around 120 μm to avoid support structures for the sensor, which would introduce dead areas and inactive material within the beam. The technology available at the moment for standard LGADs does not allow to have a 200 μm pitch sensor with a fill factor over 80% [19], so it is necessary to exploit one of the recent LGAD technologies such as AC-LGADs [20], Trench insulated LGADs [21] or Deep-Junction LGADs [22]. Prototype AC-LGADs produced at BNL are shown in fig. 3. The best estimate at present for the sensor thickness is around 120 μm to avoid support structures for the sensor, which would introduce dead area. Such a sensor could separate a single hit from two overlapping hits if they arrive more than 1.5 ns apart. The time resolution on the rising edge should be about 100 ps for the minimum ionizing signals to much better time resolution for large π/μ signals. A 2-sided readout sensor prototype is also being produced to allow X and Y position measurement for each plane.

In addition to the baseline design, an alternative design based on standard silicon sensors (PIN), is being explored by the collaboration. Compared to the LGAD technology, the PIN does not have complications associated with the gain mechanism. As a result, the signal in PIN is also smaller, which requires dedicated low-noise electronics to reach desired signal-to-noise ratios.

5. Sensor characterization

AC-LGADs overcome the granularity limitation of traditional LGADs and have been shown to provide a spatial resolution of the order of tens of μm [23]. AC-LGAD design also allows having a completely active sensor with no dead regions. Several prototypes produced by BNL were tested with many geometric configurations; an example of the sensors is shown in Fig. 3. The sensors have been tested with a laboratory IR laser TCT station [24] and at a Fermilab (FNAL) test beam [25].

The position resolution was evaluated for a few different geometries as seen in fig. 4, Left. The position resolution in the direction perpendicular to the strip direction for the studied devices goes from 10 μm to 50 μm across the entire sensor, with the maximum precision at the center between two strips. This corresponds to a precision that is a factor of 10 to 30 than the sensor pitch. What is concluded is that the pitch of 200 μm shows a better precision than the 300 μm and 500 μm devices; however, there's not much gain in position resolution with the lower pitch of 100 μm. Therefore the baseline design of 200 μm pitch strips is, at the moment, confirmed for the ATAR.

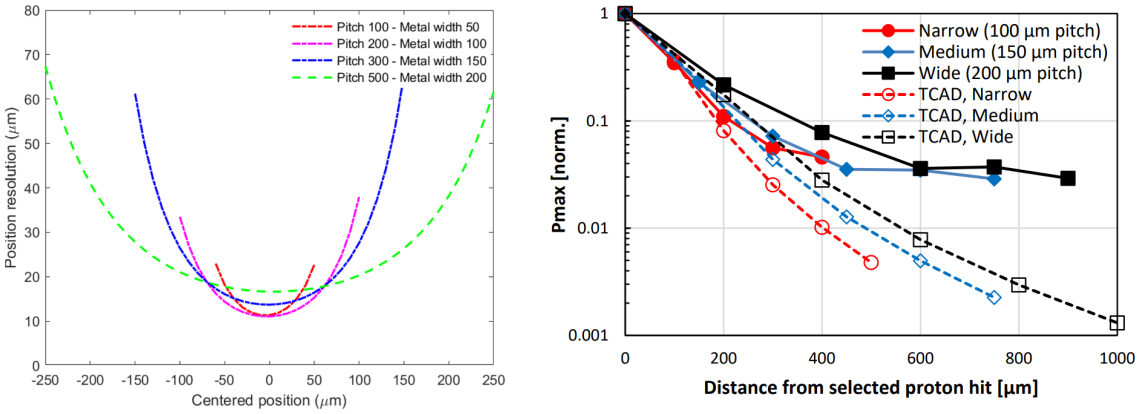

Figure 4: Left: position resolution as a function of position around the center between readout strips for the four different pitches in fig. 3. Right: logarithmic charge sharing profile for a multi-pitch BNL strip sensor (200 μm, 150 μm, 100 μm), comparison of FNAL test beam data (solid) and TCAD simulation.

The charge sharing mechanism at large distances was studied at the FNAL test beam facility, as seen in fig. 4, Right. The charge sharing profile for a multi-pitch BNL strip sensor (200 μm, 150 μm, 100 μm) is shown for test beam data and TCAD simulation (see next section). The charge sharing is expected, from the simulation, to be $< 1\%$ for distances over 600 μm from the hit. However, in the data, the charge sharing plateaus at a 3-5% level even after 1 mm of distance. This behavior is worrisome for PIONEER where a large charge deposition (100s of MIP) can cover the positron (MIP) signal at long distances. More studies on prototypes are foreseen to understand this behavior and minimize the effect.

The relation between charge sharing and strip length was also studied, as seen in fig. 5; the study is made using a laser TCT system. As seen in the plots, a sensor with longer strips has increased charge sharing. The best performance for AC-LGADs is in the case of charge not exceeding the first neighbor; this way, the signal-to-noise ratio is maximized in the position calculation. Since the ATAR will employ 2 cm long strips, the sensor design has to be adjusted to limit the charge

sharing. This can be done by increasing the N+ layer resistivity; this effect was studied with TCAD simulations, as seen in the next section.

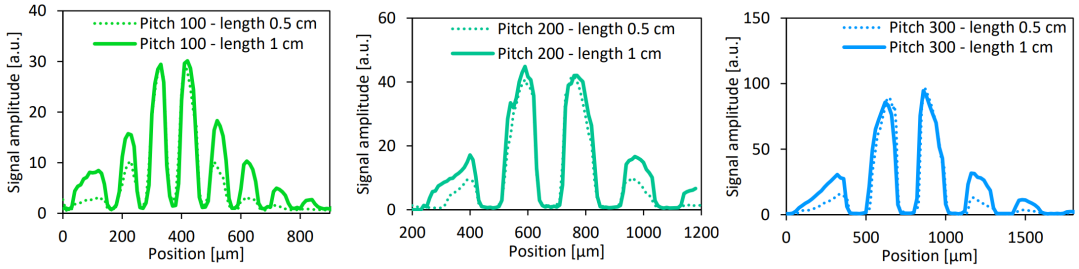

Figure 5: Effect of strip length for the geometry of the left sensor on Fig. 3, two sensors with identical geometry but different lengths are shown in the plot.

5.1 TCAD simulation.

The behavior of AC-LGADs was studied using TCAD Sentaurus and Silvaco software. The TCAD Silvaco simulation is 2D approximated, while the TCAD Sentaurus simulation uses full 3D simulation. The relation between charge sharing and N+ layer resistivities is shown in fig. 6, Left, with a study made with TCAD Silvaco. In the same plot, a comparison with data taken at the FNAL test beam for a sensor with the same geometry is shown. As expected, an increased resistivity reduces the charge-sharing profile; therefore, a more resistive layer is recommended for the prototype fabrication.

In fig. 6, Right, a TCAD Sentaurus simulation is shown for the same geometry but different strip lengths. The simulation confirms the results from the shown data in fig. 5: charge sharing is increased for longer strips. In fig. 7, TCAD simulations for 50 μm and 120 μm strip AC-LGADs are shown, and the simulation predicts larger charge sharing for thicker sensors. Therefore, for the baseline design of the ATAR, 120 μm, and 2 cm strips, a high resistivity N+ is necessary. The input of the TCAD simulation will be used to steer the BNL prototype production.

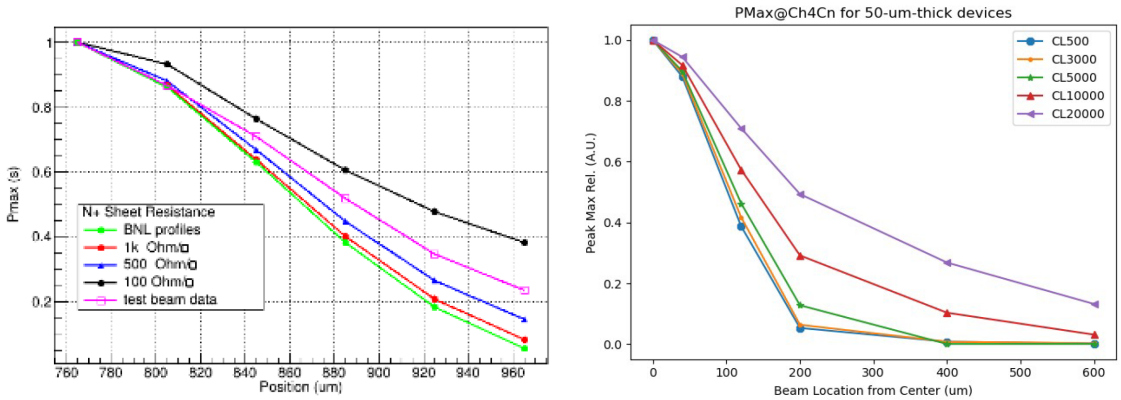

Figure 6: Left: TCAD Silvaco simulation of charge sharing profile for different N+ resistivity. Right: TCAD Sentaurus 3D simulation of charge sharing profile for different strip lengths.

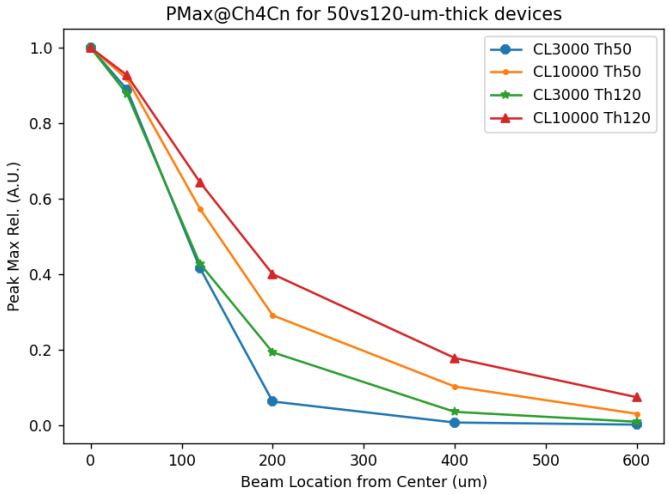

Figure 7: TCAD Sentaurus simulation of charge sharing profile for different substrate thicknesses and strip lengths. The strips have a pitch of 200 μm and a width of 80 μm. The values are normalized to the strip that is read out at position 0 μm.

5.2 Other DC-LGAD alternatives.

Alternative sensor technologies, still based on LGADs, are being evaluated for the ATAR. Trench Isolated (TI) LGADs are a novel silicon sensor technology that utilizes a deep narrow trench to electrically isolate neighboring pixels to prevent breakdown, as opposed to standard LGADs, which use a junction termination extension to prevent breakdown at the pixel edges. By utilizing the deep trench isolation technology, the no-gain region is reduced to a few micrometers, thus achieving a higher fill factor than regular LGADs. Prototype TI-LGADs sensors from Fondazione Bruno Kessler (FBK) [21] were studied at UCSC, and the inter-pad region between strips is only a few microns. This allows having a 200 μm pitch sensor with a minimal dead area.

DJ-LGADs [22] are instead based on the concept of a buried gain layer. Thanks to the buried gain layer, the pixelization of the top electrodes can be as fine as a regular silicon detector. Results from a prototype production done at CACTUS material in collaboration with UCSC and BNL show that the IP region is only a few microns for DJ-LGADs [26], making it a feasible technology for the ATAR as well.

5.3 Gain suppression (TCAD+Alpha).

The gain suppression mechanism was studied using an Am256 alpha source, injecting about 4 MeV of energy (corresponding to about 100 MIPs) in the Silicon sensor at a depth of roughly 20 μm. The setup is placed in a vacuum chamber built at UCSC for this purpose. In Fig. 8, Left, the resulting gain for an HPK-3.1 sensor is shown compared to data taken with an Sr90 beta source (MIP electrons). The gain is calculated by measuring with the same technique PiN sensors with the same geometry as the LGAD. The study is still ongoing; the plan is to use a collimator to limit the incidence angle of the alpha particle. A system to rotate the sensor and study the gain suppression as a function of injection angle is also foreseen.

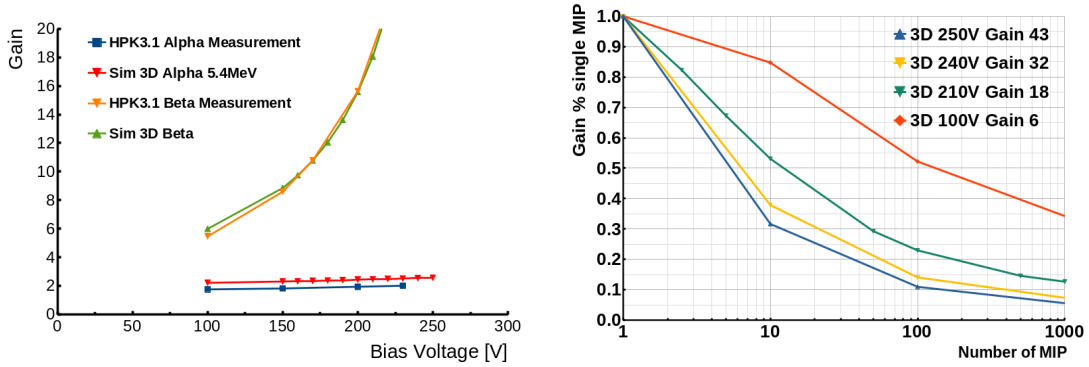

Figure 8: Left: Gain difference in an HPK sensor for beta (MIP) and alpha (about 100 MIPs) particles for data and TCAD simulation as a function of bias voltage. Right: TCAD Sentaurus simulation of Gain suppression vs number of MIPs for different gain levels.

In Fig. 8, Right, the gain suppression simulated with TCAD Sentaurus as a function of the number of MIPs injected is shown for the same HPK-3.1 device at different gain levels. It can be seen that for low gain (e.g. 6), the suppression is 50% for 100 MIPs; instead, if the device is run at high gain (e.g. 30), the suppression can be up to a factor 10. The simulation roughly confirms the results taken with the alpha source as seen in Fig. 8, Left. Therefore a recommendation for the ATAR is to employ sensors with low gain (5-15). To minimize the gain saturation effect in the ATAR several sensor prototypes with different gain layer doping profiles and geometries will be studied with the alpha source. Furthermore, the TCAD simulation will allow the testing of different gain layer configurations. The goal of this two-prong study is to find a sensor design to minimize the gain saturation.

6. Readout flex, ASIC and digitization

6.1 Flex

A short flex prototype run was made with the collaboration of UCSC and UW. The purpose was to study the effect of the flex cable on the sensor signal. The flex was interposed between an AC-LGAD sensor and an analog readout board (fig. 9, Left) and compared with direct bonding between the board and sensor. Prototype flexes with lengths of 3-7 cm were produced with 200 μm and 500 μm trace pitch. The first observation was that bonding a sensor directly to the flex cable is mechanically challenging; therefore, a proper bonding procedure must be developed.

While the signal from the sensor does not seem to be affected, the charge sharing with neighboring strips and baseline noise of channels are increased when connected to the flex. The long-range pick-up was also observed from AC-LGAD strips connected to the flex as seen in fig. 9, Right. Attempts were made to reduce the pick-up: spacing connections further apart and grounding traces in between. Only a slight improvement was observed.

The flex was also studied with a probe and with the sensor disconnected. The probe injects an LGAD-like signal in the various traces. This allows the decoupling of the flex effect from the charge sharing of AC-LGADs. The pulses from the trace where the signal is injected and the neighbors

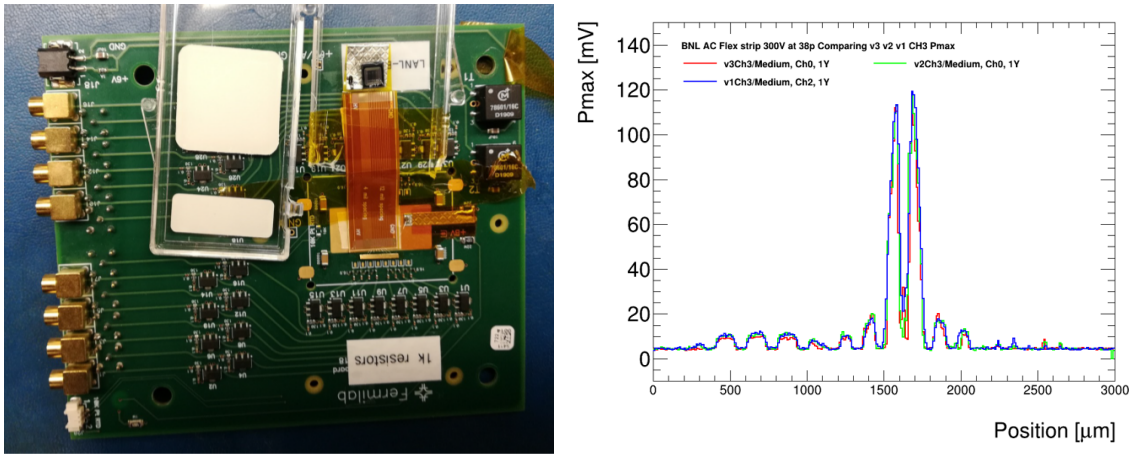

Figure 9: Left: Flex testing setup. Right: Charge sharing profile for the AC-LGAD connected to the flex for three different configurations. The strip that is read out is at position 1600 μm; the charge sharing around it is affected in a minor way. A few strips are connected to the flex between 500 μm and 1000 μm and induce cross-talk in the readout strip (blue line). To reduce the effect, the connections were spaced further apart (green line), and the traces in between were grounded (red line); a slight improvement can be seen.

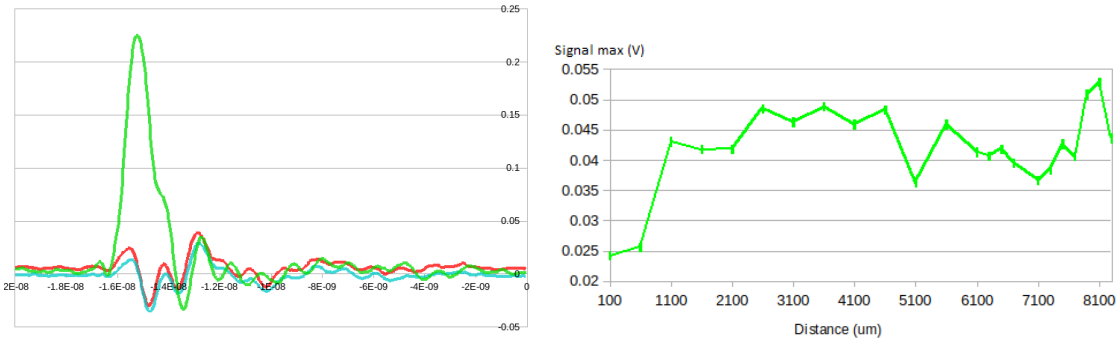

Figure 10: Left: signal injected by the probe on a trace (green) and signal picked up on the same trace when the signal is injected in the neighboring traces (blue and red). Right: response of a trace of the flex when the signal is injected in all the other traces; the response is roughly constant. The first two traces on the left are floating, and the cross-talk is less.

can be seen in fig. 10, Right. In fig. 10, Left, the signal max of the response of a trace in the center of the flex is shown with signal injected in all other traces. It can be seen that the effect is roughly constant except for the first two traces that are left floating. The study concludes that a flex re-design with a better ground connection is needed; the design can be aided by simulation software (e.g., Hyperlinx software).

6.2 ASIC and digitizer

For the analog readout, two chips were characterized at UCSC: FAST2 [27] analog (INFN Torino) and HP-SoC [28] (NALU scientific). Both chips have promising performance in terms of bandwidth a full charge collection time, HP-SoC has better performance, but it's still in the prototype stage. Both chips would not fully cover the entire dynamic range of the ATAR; a tentative solution

to the high dynamic range is to have each channel split between a high gain and low gain stage to cover the full dynamic range. This is possible since each FAST2 channel can be set with three different gain configurations; this capability is currently under study. A new readout board based on FAST2 analog is being designed to allow multiple planes of sensors to be put close together to build a prototype version of the ATAR.

A digitizer chip, HD-SoC [29], from NALU scientific is currently being evaluated. HD-SoC has 32 channels (64 channels in the next iteration) and 1 Gs/s with a complex triggering scheme. The HD-SoC chip is mounted on an evaluation board with MMCX connectors as input, and the digital communication between the chip and the NaluScope software is made through USB with an FPGA board. The characteristic of the HP-SoC chip would be satisfactory for the ATAR, a collaboration with NALU scientific is ongoing to adjust the design for PIONEER.

7. ATAR v0.5

The current short-term plan is to build a v0.5 of the PIONEER experiment to take data at PSI by 2027, which corresponds to the PSI shutdown. A limited-scale ATAR prototype is envisioned, with 10 layers and 16 channels per layer (corresponding to the FAST2 analog channels per chip). After the ATAR prototype, a small Calorimeter with limited acceptance will be placed. The first ATAR prototype will be ready and tested in a beamline at PSI by 2025.

The sensors for this prototype are being produced at BNL; they will be 120 μm thick and without a support wafer. Ten layers of these sensors will allow seeing the muon decay (traveling about 1 mm) in the ATAR prototype. The prototype readout would be based on the FAST3 analog chip (expected delivery Q1 2023) mounted on a board being designed from a collaboration of UW and UCSC. Such a board would allow having several sensors (produced in the BNL fabrication) close together with a limited number of channels per plane. The digitization would be for each channel for each event using either the HD-SoC chip or wave-dream boards.

8. Conclusions

The PIONEER experiment will provide the best measurement to date for $R_{e/\mu}$ and pion beta decay, improving by one order of magnitude the measurements of PIENU, PEN, and PIBETA. To achieve this goal, PIONEER will feature a high granularity calorimeter with high energy resolution and a fully silicon active target. The ATAR will allow reconstructing, event by event; the pion decay processes thanks to the high granularity and fast collection time. Several challenges will be faced for the ATAR design: high dynamic range, clear temporal pulse separation, full digitization, and the necessity of low dead material all around.

Many prototype devices for the baseline sensor technology, AC-LGADs, were tested at UCSC and the behavior of the charge-sharing mechanism was better understood. On top of device testing, TCAD simulations were run to model the sensor behavior and provide guidance for prototype fabrication. The relation between the charge-sharing mechanism and strip geometry was tested and simulated in 50 μm thick devices for different pitches, widths, and lengths. The behavior of 120 μm thick devices, ATAR's baseline, was simulated with TCAD software as well. The gain suppression mechanism was studied using alpha particles in a vacuum and TCAD simulation.

As a conclusion of sensors studies in the past year, a few key points are concluded for LGADs and AC-LGADs in the ATAR:

- AC-LGAD strips with 200 μm of pitch are a good choice in terms of position resolution.
- The N+ resistivity needs to be increased, especially for 120 μm devices to reduce charge-sharing. The long-range charge-sharing needs to be minimized.
- Devices running at a low gain (5-10) are better for the ATAR in terms of energy resolution and gain suppression.

For the analog readout, two chips were characterized: the FAST2 [27] analog (INFN Torino) and HP-SoC [28] (NALU scientific) chips. A flex prototype for the ATAR was produced and studied, the signal coming from the sensor is not particularly affected by the flex, however, long-range pick-up is observed. A new flex will be designed to minimize the pick-up with the lessons learned from the first prototype run and simulation inputs. A digitizer chip, HD-SoC, from NALU scientific is currently being evaluated. HD-SoC has 32 channels (64 channels in the next iteration) and 1 Gs/s with a complex triggering scheme. Finally, the first ATAR prototype is being designed with a simple readout and limited acceptance with the goal to run at PSI by 2027.

9. Acknowledgments

This work was supported by the United States Department of Energy, grant DE-FG02-04ER41286, and partially performed within the CERN RD50 collaboration.

References

[1] PIONEER collaboration, W. Altmannshofer et al., *PIONEER: Studies of Rare Pion Decays*, 2203.01981.

[2] PIONEER collaboration, S. M. Mazza, *An LGAD-Based Full Active Target for the PIONEER Experiment*, *Instruments* **5** (2021) 40, [2111.05375].

[3] "Pienu, https://pienu.triumf.ca/."

[4] "Pen, https://inspirehep.net/experiments/1511062."

[5] "Pibeta, https://inspirehep.net/experiments/1108722."

[6] V. Cirigliano and I. Rosell, *Two-loop effective theory analysis of $\pi(K) \to e\bar{\nu}_e(\gamma)$ branching ratios*, *Phys. Rev. Lett.* **99** (2007) 231801, [0707.3439].

[7] V. Cirigliano and I. Rosell, *$\pi/K \to e\bar{\nu}_e$ branching ratios to $O(e^2p^4)$ in Chiral Perturbation Theory*, *JHEP* **10** (2007) 005, [0707.4464].

[8] D. Bryman, W. J. Marciano, R. Tschirhart and T. Yamanaka, *Rare kaon and pion decays: Incisive probes for new physics beyond the standard model*, *Ann. Rev. Nucl. Part. Sci.* **61** (2011) 331–354.

[9] PIENU collaboration, A. Aguilar-Arevalo et al., *Improved Measurement of the $\pi \to e\nu$ Branching Ratio*, *Phys. Rev. Lett.* **115** (2015) 071801, [1506.05845].

[10] N. Cabibbo, *Unitary Symmetry and Leptonic Decays*, *Phys. Rev. Lett.* **10** (1963) 531–533.

[11] M. Kobayashi and T. Maskawa, *CP Violation in the Renormalizable Theory of Weak Interaction*, *Prog. Theor. Phys.* **49** (1973) 652–657.

[12] A. Czarnecki, W. J. Marciano and A. Sirlin, *Pion beta decay and Cabibbo-Kobayashi-Maskawa unitarity*, *Phys. Rev. D* **101** (2020) 091301, [1911.04685].

[13] E. Frlež et al., *Design, commissioning and performance of the PIBETA detector at PSI*, *Nucl. Instrum. Meth. A* **526** (2004) 300–347, [hep-ex/0312017].

[14] D. Pocanic et al., *Precise measurement of the $\pi^+ \to \pi^0 e^+ \nu$ branching ratio*, *Phys. Rev. Lett.* **93** (2004) 181803, [hep-ex/0312030].

[15] MEG collaboration, A. M. Baldini et al., *Search for the lepton flavour violating decay $\mu^+ \to e^+\gamma$ with the full dataset of the MEG experiment*, *Eur. Phys. J. C* **76** (2016) 434, [1605.05081].

[16] X. Qian, C. Zhang, B. Viren and M. Diwan, *Three-dimensional Imaging for Large LArTPCs*, *JINST* **13** (2018) P05032, [1803.04850].

[17] MicroBooNE collaboration, P. Abratenko et al., *Wire-cell 3D pattern recognition techniques for neutrino event reconstruction in large LArTPCs: algorithm description and quantitative evaluation with MicroBooNE simulation*, *JINST* **17** (2022) P01037, [2110.13961].

[18] G. Pellegrini et al., *Technology developments and first measurements of Low Gain Avalanche Detectors (LGAD) for high energy physics applications*, *Nucl. Instrum. Meth.* **A765** (2014) 12 – 16.

[19] ATLAS collaboration, *Technical Design Report: A High-Granularity Timing Detector for the ATLAS Phase-II Upgrade*, tech. rep., CERN, Geneva, Jun, 2020.

[20] A. Apresyan, W. Chen, G. D'Amen, K. F. Di Petrillo, G. Giacomini, R. Heller et al., *Measurements of an AC-LGAD strip sensor with a 120 GeV proton beam*, *JINST* **15** (2020) P09038, [2006.01999].

[21] G. Paternoster, G. Borghi, M. Boscardin, N. Cartiglia, M. Ferrero, F. Ficorella et al., *Trench-isolated low gain avalanche diodes (ti-lgads)*, *IEEE Electron Device Letters* **41** (2020) 884–887.

[22] S. Ayyoub, C. Gee, R. Islam, S. M. Mazza, B. Schumm, A. Seiden et al., *A new approach to achieving high granularity for silicon diode detectors with impact ionization gain*, 2101.00511.

[23] M. Tornago, R. Arcidiacono, N. Cartiglia, M. Costa, M. Ferrero, M. Mandurrino et al., *Resistive ac-coupled silicon detectors: Principles of operation and first results from a combined analysis of beam test and laser data*, *Nuclear Instruments and Methods in Physics Research Section A: Accelerators, Spectrometers, Detectors and Associated Equipment* **1003** (2021) 165319.

[24] Particulars-TCT, "https://http://particulars.si/."

[25] "Development of ac-lgads for high-rate particle detection, https://indico.cern.ch/event/861104/contributions/4503072/."

[26] "Deep junction lgad: a new approach to high granularity lgad, https://indico.cern.ch/event/1132520/contributions/5140036/."

[27] E. Olave, F. Fausti, N. Cartiglia, R. Arcidiacono, H.-W. Sadrozinski and A. Seiden, *Design and characterization of the fast chip: a front-end for 4d tracking systems based on ultra-fast silicon detectors aiming at 30 ps time resolution*, *Nuclear Instruments and Methods in Physics Research Section A: Accelerators, Spectrometers, Detectors and Associated Equipment* **985** (2021) 164615.

[28] C. Chock et al., *First test results of the trans-impedance amplifier stage of the ultra-fast HPSoC ASIC*, *JINST* **18** (2023) C02016, [2210.09555].

[29] Nalu Scientific. https://www.sbir.gov/sbirsearch/detail/2103931.